Results in Engineering 30 (2026) 110561

Contents lists available at ScienceDirect

Results in Engineering

journal homepage: www.sciencedirect.com/journal/results-in-engineering

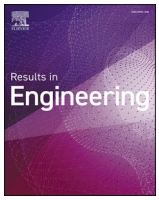

Research paper

Stochastic parametric LCA of GHG footprints of hyperloop systems

Jianxiang Ma [a,*], Jianpeng Cao [b,d], Lorenzo Benedetti [c], Zienab Elghoul [c], Guillaume Habert [a]

[a] Chair of Sustainable Construction, Institute of Construction and Infrastructure Management, ETH Zürich, Stefano-Franscini-Platz 5, 8093 Zurich, Switzerland
[b] Faculty of Architecture, Department of Real Estate and Construction, The University of Hong Kong, Pokfulam, Hong Kong SAR, China
[c] EuroTube Foundation, Neugutstrasse 66, 8600 Dübendorf, Switzerland
[d] Faculty of Architecture & the Built Environment, Delft University of Technology, Julianalaan 134, 2628 BZ Delft, Netherlands

ARTICLE INFO

Keywords:
Emission uncertainty
Vacuum transport
Integrated impact assessment
Stakeholder contribution
Prospective mobility

ABSTRACT

Hyperloop systems offer high-speed, low-emission transport, yet existing life-cycle assessments (LCA) report inconsistent greenhouse gas (GHG) results because of differing system boundaries and assumptions. This study introduces a stochastic parametric LCA framework that quantifies both expected GHG emissions and associated uncertainties across four hyperloop configurations. A unified variance-decomposition model captures uncertainty arising from both design-type decisions and cross-design parameters, and maps these to stakeholder groups. Applied to a Zurich–Geneva case study, results show that tube material has the greatest impact on mean emissions, while component service life is the largest single source of uncertainty and operational parameters collectively contribute the second-largest share. Among stakeholders, operators have the greatest influence on GHG footprint by controlling most of the operational parameters and affecting component lifespans through maintenance. Infrastructure designers show the second greatest influence, primarily via their decision between using concrete or steel tubes. Pod designers rank third by determining the levitation technology and pod design characteristics, while constructors have the least influence, with their most impactful decision being the selection of material suppliers. This decision-centric framework enables transparent evaluation of carbon impacts and uncertainty and supports sustainable infrastructure planning for next-generation transport systems.

1. Introduction

Global transport demand is rising with population and industrial growth. In 2022, transport accounted for over one-third of end-use GHG emissions and continues to expand with increased air travel [1,2]. Aviation decarbonization remains slow due to the limited scalability of Sustainable Aviation Fuels and the infeasibility of current battery technologies for electric aircraft [3,4].

Hyperloop, a vacuum-based maglev system, has emerged as a promising low-carbon alternative to short-haul flights. With speeds exceeding 1000 km/h, it offers a feasible pathway for decarbonized high-speed travel that only requires half the battery density compared to electric aircraft [5–7]. A typical hyperloop consists of a low-pressure tube, maglev-powered pods, and supporting infrastructure.

Fig. 1 illustrates the hyperloop infrastructure proposed by EuroTube [8]. Hyperloop infrastructure mainly comprises three component types: structural components, electrical components, and vacuum components. The primary structural components consist of sealed tubes supported by pillars, connection joints between the tubes, and rails for pod movement. The electrical components are responsible for power transfer and signal transmission. Vacuum components, such as the liner, airlocks, valves, and pumps, maintain low-pressure conditions essential for efficient operation. The airlock serves as a terminal section that allows pods to enter and exit while preventing atmospheric air from entering, thereby ensuring both efficiency and safety. Vacuum pumps reduce air pressure in the airlock to operational levels for each departure and compensate for vacuum losses caused by infrastructure leakage.

Although several studies have evaluated hyperloop's environmental performance, comparative GHG footprints across design types remain unexamined. Existing systems differ mainly in tube material and levitation technology. As shown in Fig. 2, the Electrodynamic Suspension (EDS) system relies motion-induced eddy currents in the conductive rails for magnetic repulsion, whereas the Electromagnetic Suspension (EMS) relies on continuous attraction between onboard electromagnets and the ferromagnetic tracks.

Hyperloop pods use linear motors for propulsion while levitating. EDS systems typically adopt Linear Induction Motors (LIMs), which induce magnetic fields in aluminum rails but suffer efficiency losses due

* Corresponding author.
E-mail address: ma@ibi.baug.ethz.ch (J. Ma).

https://doi.org/10.1016/j.rineng.2026.110561
Received 26 August 2025; Received in revised form 3 February 2026; Accepted 15 April 2026
Available online 17 April 2026

to slip and reactance. EMS systems use Linear Synchronous Reluctance Motors (LSRMs), offering higher efficiency and lower cost using ferromagnetic rails, but requiring precise control. This study assumes EDS with LIMs and EMS with LSRMs to avoid mixed rail materials, which would increase both cost and emissions. Tube materials, such as concrete and steel, also significantly affect system environmental performance [5,6,9,10]. Concrete offers high durability but requires an internal liner to ensure airtightness, whereas steel naturally provides superior sealing capabilities although it is susceptible to corrosion.

Given these diverse design options for hyperloop systems, Life Cycle Assessment (LCA) is essential for evaluating their environmental performance of hyperloop systems across their entire life cycles [11–13]. LCA enables quantitative comparison of alternative designs under an identical functional unit and scope, thus further guiding decisions for decarbonization. While several studies have assessed hyperloop emissions, most have focused on a single design configuration and have yielded conflicting conclusions due to inconsistent boundaries and assumptions. Moreover, no study to date has systematically compared the four major hyperloop design types within a unified framework that incorporates uncertainty. To address this gap, we develop a stochastic parametric LCA framework with unified boundaries and assumptions and apply it to four technically feasible configurations defined by levitation technology and tube material. The levitation technology determines the rail materials: the EDS system needs a conductive reaction rail, represented here by aluminum, whereas the EMS system relies on a ferromagnetic rail, represented here by steel. Accordingly, we evaluate four configurations:

(1) EDS with concrete tubes and aluminum rails (EDS-CT),
(2) EDS with steel tubes and aluminum rails (EDS-ST),
(3) EMS with concrete tubes and steel rails (EMS-CT),
(4) EMS with steel tubes and steel rails (EMS-ST).

2. Literature review

GHG emissions from public transport systems arise primarily from infrastructures and operations. Infrastructure emissions depend on material choices and component service life, while operational emissions are shaped by the energy source and passenger occupancy [14–16]. In emerging systems like hyperloop, infrastructure and operations are more tightly coupled than in conventional rail systems. The choice of pod levitation technology influences infrastructure emissions by determining the required rail material and affects operational emissions through differences in energy demands by propulsion and internal cooling between EMS and EDS systems. These interdependencies underscore the need for holistic LCA models that jointly assess both embodied and operational carbon emissions to support informed design and decarbonization of emerging transport systems.

Since the vacuum transportation concept was popularized by Elon Musk [17], several studies have assessed the environmental performance of hyperloop designs. Janić [18] compared direct energy use and GHG emissions of high-speed railways (HSR), Transrapid Maglev (TRM), and an EMS hyperloop on the Moscow–St. Petersburg route. His results indicate that the hyperloop system has the best economic and environmental performance followed by TRM and HSR. Later in 2021, Janić [19] extended this work by developing an analytical mechanical energy consumption model under multiple operating scenarios for HSR, TRM, and EMS hyperloop, showing that emissions were shaped by journey distance and seat capacity. However, both studies focus solely on operational impacts and exclude infrastructure-related emissions.

Hirde et al. [20] proposed a framework to evaluate the construction and operational GHG footprints of an EMS-CT hyperloop across three routes: Mumba–Pune, Dubai–Abu Dhabi, and Chicago–Pittsburgh. They found that while hyperloop is 40 % more energy-efficient than aviation, it consumes more energy than TRM and HSR. Its infrastructure-related GHG emissions also exceed those of aviation by 61 %. Nevertheless, hyperloop's overall GHG footprint can still be lower than aviation if it ispowered by a clean electricity mix.

More recently, Beckert et al. [5] conducted a comprehensive LCA of an EDS-CT hyperloop system between Zurich and Geneva, covering both embodied infrastructure emissions and pod operations. Their analysis shows that hyperloop closely resembles HSR, while offering aviation-like speeds. The included local sensitivity analysis of operational parameters illustrates that vacuum pressure, the block ratio of the infrastructure, and the pod passenger capacity are the most influential parameters affecting the operational energy consumption.

Despite recent progress, existing studies report conflicting conclusions regarding hyperloop's emissions potential: Beckert et al. [5] suggested values comparable to HSR, whereas Hirde et al. [20] projected emissions up to three times higher. This discrepancy stems mainly from divergent assumptions in the LCA models. For example, Beckert et al. assumed a 100-year service life for the main structural components, whereas Hirde et al. used a 40-year assumption. Since hyperloop remains a technology under development, such assumptions introduce considerable uncertainty that deterministic LCAs cannot capture, limiting their supporting for comprehensive design phase decisions [21].

While local sensitivity analyses can evaluate the impact of individual parameters, they cannot capture the overall uncertainty arising from simultaneous variation in multiple parameters. Stochastic LCA is therefore needed to assess the combined effects of all inputs for hyperloop systems. These inputs fall into two categories: cross-design

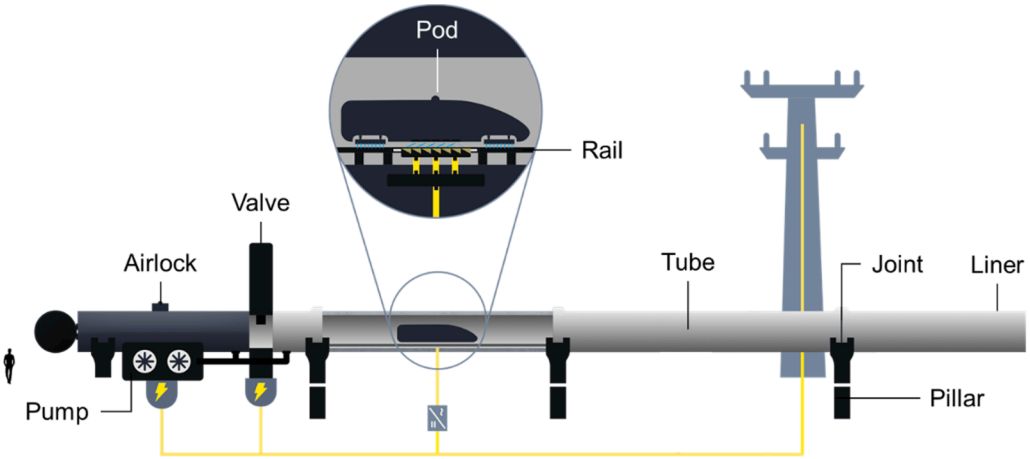

Fig. 1. Schematic illustration of hyperloop transportation system from EuroTube [8].

parameters, which are shared across all configurations (e.g., vacuum pressure), and design-type decisions, which define the system architecture (e.g., levitation technology). To further compare the influence of design-type decisions with that of cross-design variability, we propose a unified framework that integrates multiple stochastic LCAs, quantifies the contributions of both parameter types, and further links them to the responsible stakeholders to better inform decision-making.

3. Materials and methods

Fig. 3 presents our stochastic parametric LCA framework. We classify uncertainty into two categories. Design-type decisions are categorical choices among hyperloop types, and cross-design parameters are continuous inputs shared across all types. For each design type, we assign probability distributions to the cross-design parameters and run Monte Carlo (MC) simulations to generate GHG outcomes across the covered LCA stages. We then fit Polynomial Chaos Expansion (PCE) surrogates to the MC samples and apply Sobol' decomposition to attribute variance to cross-design parameters. These variances are then averaged across all the design types to represent their influence across the four types of hyperloop designs. To quantify the uncertainty impact of design-type decisions, we regroup the MC outputs by design type and calculate the design-type variance of mean GHG emissions. Finally, we map the variances associated with both design-type decisions and cross-design parameters to stakeholder groups to quantify how each group's choices shape the hyperloop system's GHG footprint.

3.1. Goal and scope

The aim of this study is to quantify and compare the GHG footprint of four hyperloop designs at the midpoint level, identify the key parameters with the highest uncertainty contributions, and further estimate the influence of decisions made by various stakeholders. The functional unit is the transportof one passenger over 1 km by hyperloop over a 100-year system lifetime, with demand modeled on the Zurich–Geneva route. The LCA scope follows the European standard DIN EN 15,978:2012–10 [22] and covers the product stage (A1–A3), the construction stage (A4–A5), the replacement subphase (B4), and the operational energy subphase (B6). We model replacement subphase through service-life-based annualization of embodied impacts using component service-life distributions, and we Ndocument the full modeling assumptions and formulas in Section S1 in the supplementary material. Due to limited data availability, this study does not include the embodied emissions of the pod or pod-related maintenance activities.

3.2. Life cycle inventory

Life cycle inventory analysis quantifies all inputs and outputs of the studied system. Foreground data, including the parameters associated with uncertainties, are based on the literature and on expert assumptions from EuroTube. Background data, consisting of embodied impacts of materials and energy sources, are extracted from ecoinvent 3.10.1 using the cut-off allocation method [23].

Table 1 summarizes the four hyperloop designs. EDS configurations use aluminum rails and pod-side LIMs, whereas EMS configurations use steel rails and pod-side LSRMs. Concrete tubes require internal liners to achieve a leakage rate in the range of 0.001 to 0.01 Pa·L/s per m^3; while, steel tubes naturally achieve a smaller leakage rate below 0.001 Pa·L/s per m^3 and therefore do not require liners [20,24]. All designs share a 4.4 m inner tube diameter with a block ratio of 0.6. Each 20 m tube segment is connected via silicone joints and supported by two pillars at both ends (Fig. 1). Other infrastructure parameters are identical across the four hyperloop design types.

3.3. Life cycle impact assessment

As this study focuses on the GHG emissions of hyperloops, for the Life Cycle Impact Assessment (LCIA) stage, we used the Global Warming Potential over a 100-year time horizon (GWP100), with characterization factors from the Intergovernmental Panel on Climate Change (IPCC) Sixth Assessment Report [25]. We averaged the GHG emissions from each covered LCA stage by the estimated annual number of transported passengers between Zurich and Geneva. The detailed system model is described in Section S1 the supplementary material.

3.3.1. Product stage

In the product stage, we estimated the distributions of embodied GHG emissions for infrastructure components using MC simulations with uncertainty data from the ecoinvent 3.10.1 database. In ecoinvent, the uncertainty of an emission factor is characterized by a pedigree matrix, which describes the uncertainty of a process across five dimensions: reliability, completeness, temporal correlation, geographical correlation, and technological correlation [26,27]. Scores for these dimensions are automatically translated into statistical factors by the Brightway 2.5 Python package [28] for running MC simulations to obtain the GHG emissions distributions. The quantities of materials for the four hyperloop designs are provided in Table S1 in the supplementary material.

3.3.2. Construction stage

Existing literature indicates that the construction stage contributes only a small proportion of the total GHG emissions in linear transportation infrastructures, despite the complexity of construction activities [14,29–32]. To simplify this analysis, we categorized construction emissions into three groups: prefabrication, transportation, and on-site construction. We modeled each group as a probability distribution derived from MC simulation based on energy consumption from the machines used in the construction stage.

Specifically, we adopted the Smart Mobile Factory (SMF) concept to minimize emissions in the construction stage [33–35]. For

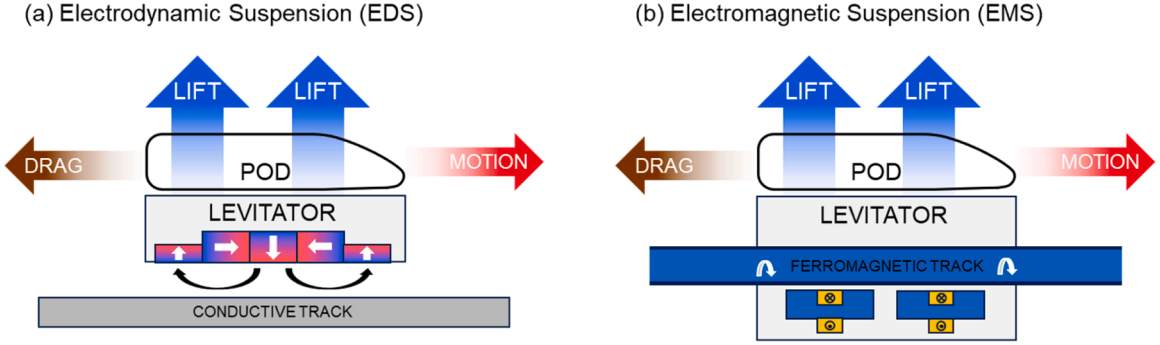

Fig. 2. Core levitation principle of maglev technology adapted from [9], (a) Electrodynamic suspension, (b) Electromagnetic suspension.

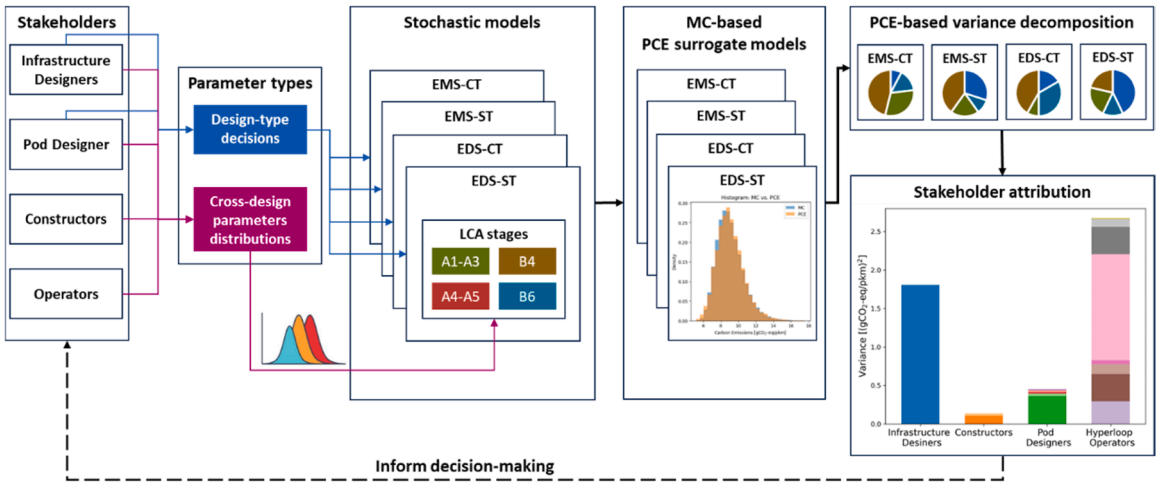

Fig. 3. Overview of the stochastic parametric LCA framework for novel transportation systems.

Table 1
Design options for four types of hyperloop design types.

Design Option	EDS-CT	EDS-ST	EMS-CT	EMS-ST
Infrastructure Parameters				
1. Tube material	Concrete	Steel	Concrete	Steel
2. Rail material	Aluminum	Aluminum	Steel	Steel
3. Liner material	Polymer	None	Polymer	None
Operation Parameters				
4. Levitation suspension	Electrodynamic	Electrodynamic	Electromagnetic	Electromagnetic
5. System leakage rate	0.001 to 0.01 Pa·L/s per m^3	0.0001 to 0.001 Pa·L/s per m^3	0.001 to 0.01 Pa·L/s per m^3	0.0001 to 0.001 Pa·L/s per m^3
6. Propulsion	Pod-side LIM	Pod-side LIM	Pod-side LSRM	Pod-side LSRM

prefabrication, the major activities include concrete mixing, casting, and tube welding, with uncertainties arising from electricity emission factors in the database and the equipment operation durations. The operation durations were modeled as uniform distributions using EuroTube's experimental production data. We modeled transportation emissions using distributions obtained from various relocation strategies [36]. Due to the lack of empirical data, we estimated the on-site construction emissions by scaling energy consumption data from high-speed railways (HSR) construction. Details of the modeling of construction energy consumption are provided in Section S3 in the supplementary material.

3.3.3. Component service life in the replacement stage

Existing studies show that the GHG footprint of transportation infrastructure is highly sensitive to component service lives, yet empirical data for hyperloop are unavailable. We therefore modeled service life as a probability distribution, using its design lifespan as the mean and the standard deviation estimated from the literature-based coefficients of variation (COV). This approach is widely used in comparative LCA studies to capture uncertainty when empirical data are lacking [15,16]. Weibull and lognormal distributions are used for their non-negativity and ease of interpretation [37–40]. We applied Weibull distributions to tubes, pillars, and rails due to their structural similarity to bridges [40–42], while we assigned lognormal distributions to vacuum components, where no empirical data exists [38]. Specifically, we assigned a 100-year lifespan to both concrete and steel tubes, with COVs of 0.25 and 0.20, respectively [43]. We extended steel rail service life to 60 years with a COV of 0.20 to reflect reduced wear under vacuum and maglev conditions and set aluminum rail service life to 50 years with a COV of 0.25 to account for the eddy current heating from LIMs. For all other components, we applied a COV of 0.20 based on literature [15,16]. To avoid overestimation, we truncated all distributions at a minimum of five years and a maximum of 1.5 times the mean.

3.3.4. Operational energy

Operational energy includes electricity consumption for vacuum and pod operations. We excluded maintenance-related energy due to limited data availability and its minimal contribution [44]. Detailed modeling is provided in Section S4 of the supplementary material.

3.3.4.1. Vacuum operation energy. Vacuum operation consists of three activities: initial evacuation, airlock operation, and vacuum assurance operation. We modeled all three activities as isothermal processes, with the airlock operation frequency determined by the number of annual pod departures required to meet the demand between Zurich and Geneva. Vacuum assurance operation energy was derived from leakage rates (see Table 1) and pressure differentials. We modeled vacuum pressure as a uniform distribution ranging from 100 to 1000 Pa and pump efficiency from 0.3 to 0.6 [20,45].

3.3.4.2. Propulsion energy modeling. To accelerate the pod, the linear motor must overcome three forces: inertia, aerodynamic drag, and electromagnetic drag. Although the low-pressure environment reduces aerodynamic friction, high speeds still induce aerodynamic drag because of choking between the pod and tube walls. This drag force stems from pressure differentials between the pod's front and rear. Computational fluid dynamics (CFD) studies demonstrate that the aerodynamic drag coefficient depends primarily on the system's block ratio and pod speed, with negligible influence from pod shape, length, or vacuum pressure [46–49]. Therefore, we estimated the aerodynamic forces by interpolating and extrapolating the coefficients at a block ratio of 0.6 from Table 2 in the supplementary material.

Electromagnetic drag depends on the levitation system: EMS uses a speed-dependent lift-to-drag ratio [20], whereas in EDS, drag depends on the square root of the inverse LIM slip speed. We assumed pod speed in EDS systems scales linearly with slip speed with a factor of 0.85 speed

Table 2
Data used in the LCA model of four hyperloop designs.

Variable	Unit	Type	Parameter	Note
Product Stage				
1. GHG emissions of concrete tube	$kgCO_2$-eq/m	Lognormal	μ: 1558.628 σ: 94.937	MC simulation based on mean and pedigree matrix from ecoinvent database
2. GHG emissions of steel tube	$kgCO_2$-eq/m	Lognormal	μ: 5737.470 σ: 396.300	
3. GHG emissions of aluminum rail	$kgCO_2$-eq/m	Lognormal	μ: 1060.229 σ: 102.048	
4. GHG emissions of steel rail	$kgCO_2$-eq/m	Lognormal	μ: 1166.008 σ: 65.845	
5. GHG emissions of pillar	$kgCO_2$-eq/m	Lognormal	μ: 311.838 σ: 19.721	
6. GHG emissions of joint	$kgCO_2$-eq/m	Lognormal	μ: 3.905 σ: 0.389	
7. GHG emissions of liner	$kgCO_2$-eq/m	Lognormal	μ: 210.419 σ: 46.187	
8. GHG emissions of valve	$kgCO_2$-eq/m	Lognormal	μ: 132.608 σ: 17.183	
9. GHG emissions of pump	$kgCO_2$-eq/m	Lognormal	μ: 29.828 σ: 3.891	
Construction Stage				
10. Transportation of EDS-CT	$kgCO_2$-eq/m	Lognormal	μ: 31.728 σ: 10.915	MC simulation based on machine power and activity duration data provided by EuroTube
11. Transportation of EDS-ST	$kgCO_2$-eq/m	Lognormal	μ: 5.364 σ: 4.795	
12. Transportation of EMS-CT	$kgCO_2$-eq/m	Lognormal	μ: 33.192 σ: 11.419	
13. Transportation of EMS-ST	$kgCO_2$-eq/m	Lognormal	μ: 5.933 σ: 5.303	
14. Prefabrication of EDS-CT	$kgCO_2$-eq/m	Lognormal	μ: 97.886 σ: 19.954	
15. Prefabrication of EDS-ST	$kgCO_2$-eq/m	Lognormal	μ: 97.267 σ: 19.960	
16. Prefabrication of EMS-CT	$kgCO_2$-eq/m	Lognormal	μ: 97.886 σ: 19.954	
17. Prefabrication of EMS-ST	$kgCO_2$-eq/m	Lognormal	μ: 97.267 σ: 19.960	
18. On-site construction of EDS-CT	$kgCO_2$-eq/m	Lognormal	μ: 935.137 σ: 195.942	
19. On-site construction of EDS-ST	$kgCO_2$-eq/m	Lognormal	μ: 402.919 σ: 92.388	
20. On-site construction of EMS-CT	$kgCO_2$-eq/m	Lognormal	μ: 935.137 σ: 195.942	
21. On-site construction of EMS-ST	$kgCO_2$-eq/m	Lognormal	μ: 402.919 σ: 92.388	
Service Life				
22. Service life of concrete tube	year	Weibull	μ: 100 σ: 25	Truncation at (5, 150), μ: [5,6,43]
23. Service life of steel tube	year	Weibull	μ: 100 σ: 20	Truncation at (5, 150), μ: [5,6,59]
24. Service life of aluminum rail	year	Weibull	μ: 50, σ: 12.5	Truncation at (5,75), μ: [5,6]
25. Service life of steel rail	year	Weibull	μ: 60 σ: 12	Truncation at (5, 90), μ extended based on [42,40]
26. Service life of pillar	year	Weibull	μ: 100 σ: 25	Truncation at (5, 150), μ from [5,6,43]
27. Service life of joint	year	Lognormal	μ: 30 σ: 6	Truncation at (5, 1.5 μ), μ from [5,6]
28. Service life of liner	year	Lognormal	μ: 60 σ: 12	
29. Service life of valve	year	Lognormal	μ: 30 σ: 6	
30. Service life of pump	year	Lognormal	μ: 12 σ: 2.4	
Vacuum Operation				
31. Vacuum pressure	Pa	Uniform	min: 100 max: 1000	Data from [5,6]
32. Concrete tube leakage rate	PaL/s per m^3	Uniform	min: 0.001 max: 0.01	Data from [24,20]
33. Steel tube leakage rate	PaL/s per m^3	Uniform	min: 0.0001 max: 0.001	
34. Vacuum pump efficiency	-	Uniform	min: 0.3 max: 0.6	
Pod Design				
35. LIM efficiency	-	Uniform	min: 0.7 max: 0.8	Data from [54,51]
36. LSRM efficiency	-	Uniform	min: 0.8 max: 0.9	Data from [60]
37. Pod mass	ton	Uniform	min: 30 max: 50	Own assumption
38. CoP of cooling system	-	Uniform	min: 2.1 max: 4	Data from [53]
39. Regenerative braking efficiency	-	Uniform	min: 0.3 max: 0.6	Data from [5,6]
40. Battery charging efficiency	-	Uniform	min: 0.85 max: 0.95	Data from [61]
41. Battery discharging efficiency	-	Uniform	min: 0.9 max: 0.95	
42. Pod share of aerodynamic heating	-	Uniform	min: 0.2 max: 0.8	Data from [5]
Pod Operation				
43. Occupancy rate	-	Uniform	min: 0.75 max: 0.85	Own assumptions based on [5,6]
44. Travel distance	km	Uniform	min: 100 max: 600	
45. Cruise speed	km/h	Uniform	min: 600 max: 1200	
46. Acceleration/ deceleration	m/s^2	Uniform	min: 0.5 max:2	
47. GHG emissions of operational electricity	$kgCO_2$-eq/ kWh	Lognormal	μ: 0.0112 σ:0.00221	MC simulation based on mean and pedigree matrix from ecoinvent

[9,50,51].

Additionally, current pod designs incorporate regenerative braking systems to recover kinetic energy during deceleration. We modeled the recovery efficiency as a uniform distribution between 0.3 and 0.6 based on [5,10].

3.3.4.3. On-board energy modeling. In this study, the pod has a floor area of 64 m^2 with 70 seats installed. The energy consumption of on-board facilities in hyperloop pods is comparable to that of fuselage systems in aviation [5,6]. Thus, we assumed the on-board facilities, including entertainment electronics and lighting, had a power at density of 18.57 W/m^2 with an average efficiency of 0.8 [52].

Aerodynamic heating and internal heat sources, such as motors and batteries, necessitate active cooling to maintain passenger comfort inside the pod. The low-vacuum tube environment limits external heat dissipation and requires a heat pump combined with phase-change material (PCM) to effectively regulate the internal temperature. We modeled the fraction of total heat reaching the pod as a uniform

distribution ranging from 20 % to 80 % [5] and assumed the coefficient of performance (COP) of the heat pump followed a uniform distribution from 2.1 to 4 [53]. Passenger heat output was fixed at 80 W/person, with occupancy modeled from 0.75 to 0.85. We modeled the motor efficiency as a uniform distribution: 0.7–0.8 for LIMs in EDS systems [51,54] and 0.8–0.9 for LSRMs in EMS systems [9]. Battery charging and discharging efficiencies were modeled as uniform distributions ranging from 0.85 to 0.95 and from 0.9 to 0.95, respectively [5,10].

3.4. Uncertainty quantification

Table 2 summarizes the input parameter distributions, including the mean μ the standard deviation σ, and their sources in the "Note" column. These distributions were incorporated into the stochastic LCA framework using the OpenTURNS Python package [55] to run the MC simulations and generate sample data for statistical analysis of the system's GHG emissions. To align the model predictions with the mean simulation outputs, we used SciPy [56] to minimize the difference between predicted and sampled means. This approach enabled consistent estimation of stage-wise GHG emissions at the mean output values.

We conducted the Sobol' variance decomposition to estimate the uncertainty contribution of each cross-design parameter to the overall uncertainty [57]. To manage the high-dimensional input space and reduce computational load, we trained PCE surrogates on the MC data. PCE expresses the output as a sum of orthogonal polynomial terms, enabling more efficient variance analysis compared to MC-based analysis [58]. Surrogate accuracy was assessed using leave-one-out (LOO) cross-validation, with a maximum allowable error of 0.05. Surrogate model performance results are reported in Section S5 of the supplementary material.

3.5. Stakeholder-attributed variance

We attributed the variance contributions from both design-type decisions and cross-design parameters to stakeholder groups to quantify how their decisions shape the hyperloop's GHG footprint. The four key stakeholder groups considered are:

- Infrastructure designers, who select tube materials and vacuum pump efficiency.
- Constructors, who manage supplier selection, prefabrication activities, transport, and on-site construction activities.
- Pod designers, who determine the levitation technology, pod mass, and subsystem efficiencies, including motor efficiency, battery efficiency, and the COP of the heat pump.
- Operators, who control operational parameters (e.g., vacuum pressure, occupancy) and influence component service lives through maintenance.

Conceptually, we treat the GHG emissions per passenger-kilometer Yas a random variable whose variability arises from two sources: (i) the discrete design-type decisions D (tube material and levitation technology) and (ii) the continuous parameters, such as component service lives, leakage rates, and subsystem efficiencies. Applying the law of total variance with respect to D, we can decompose the total variance of Y using Eq. (1),

$$Var(Y) = Var(\mathbb{E}[Y|D]) + \mathbb{E}[\mathrm{Var}(Y|D)] \tag{1}$$

where $\mathrm{Var}(\mathbb{E}[Y|D])$ represents the variance attributable to differences among design-type choices, and $\mathbb{E}[\mathrm{Var}(Y|D)]$ denotes the average variance arising from the cross-design parameters.

We approximate the design-type component $\mathrm{Var}(\mathbb{E}[Y|D])$ by assuming that the design-type decisions are independent and therefore decomposing their contributions additively, as shown in Eq. (2) below, where σ_i^2 is the variance contribution of design decision i.

$$Var(\mathbb{E}[Y|D]) = \sum_{i=1}^{n} \sigma_i^2 \tag{2}$$

For the cross-design component $\mathbb{E}[\mathrm{Var}(Y|D)]$, we first performed a Sobol'-based variance decomposition for each design type p, treating the m continuous parameters as independent of each other. For design type p, Eq. (5) decomposes the system variance,

$$Var(Y|D=p) = \sum_{j=1}^{m} \left(\sigma_j^p\right)^2 + \sigma_{\mathrm{int},p}^2 \tag{3}$$

where $\left(\sigma_j^p\right)^2$ is the main-effect variance contribution of parameter j in design type p, and $\sigma_{\mathrm{int},p}^2$ collects the higher-order interaction terms among the continuous parameters. In our numerical results, the interaction terms are several orders of magnitude smaller than the corresponding main-effect contributions, therefore, we can approximate the cross-design component $\mathbb{E}[\mathrm{Var}(Y|D)]$ by averaging the main-effect variance contributions across q design types by Eq. (4).

$$\mathbb{E}[\mathrm{Var}(Y|D)] \approx \sum_{j=1}^{m} \left(\frac{1}{q}\sum_{p=1}^{q} \left(\sigma_j^p\right)^2\right) \tag{4}$$

Taken together, we can approximate the total variance of Y using the components from design-type choices and cross-design parameters by Eq. (5),

$$Var(Y) \approx \sum_{i=1}^{n} \sigma_i^2 + \sum_{j=1}^{m}\sum_{p=1}^{q} \left(\frac{1}{q}\left(\sigma_j^p\right)^2\right) \tag{5}$$

By assigning the design-type decisions and cross-design parameters to the corresponding stakeholders, we can reformulate Eq. (5) to Eq. (6).

$$Var(Y) \approx \sum_{s\in S}\left[\sum_{i\in I_s}\sigma_i^2 + \sum_{j\in J_s}\sum_{p=1}^{q}\left(\frac{1}{q}\left(\sigma_j^p\right)^2\right)\right] \tag{6}$$

Here, S is the set of stakeholders indexed by s, and I_s and J_s denote the sets of design-type decision and cross-design parameters attributed to stakeholder s, respectively. Accordingly, we can calculate the uncertainty impact determined by stakeholder s by Eq. (7).

$$\sigma_s^2 = \sum_{i\in I_s}\sigma_i^2 + \sum_{j\in J_s}\sum_{p=1}^{q}\left(\frac{1}{q}\left(\sigma_j^p\right)^2\right) \tag{7}$$

For a given design-type decision i with l_i options, we can compute σ_i^2 from the MC outputs by regrouping the samples according to the chosen option and evaluating the between-option variance of mean outcomes using Eq. (8),

$$\sigma_i^2 = \sum_{k=1}^{l_i} w_k(\mu_k - \mu_{\mathrm{tot}})^2 \tag{8}$$

where k indexes the options, μ_k is the mean GHG emssions for option k, μ_{tot} is the mean across all options, and w_k is the probability of selecting option k. As we assumed no prior preference among the options and simulated an equal number of samples for each option, we set $w_k = 1/l_i$, so Eq. (8) simplifies to Eq. (9).

$$\sigma_i^2 = \frac{1}{l_i}\sum_{k=1}^{l_i}(\mu_k - \mu_{\mathrm{tot}})^2 \tag{9}$$

Substituting Eq. (9) into Eq. (7), the variance contribution attributed to stakeholder s can be computed using Eq. (10).

$$\sigma_s^2 = \sum_{i \in I_s} \left(\frac{1}{l_i} \sum_{k=1}^{l_i} (\mu_k - \mu_{\text{tot}})^2 \right) + \frac{1}{q} \sum_{j \in J_s} \sum_{p=1}^{q} \left(\sigma_j^p \right)^2 \quad (10)$$

By expressing variances from design-type decisions and cross-design parameters on the unified scale of the total variance $\text{Var}(Y)$, this formulation provides a consistent basis for aggregating these components and attributing them to specific stakeholder. Table 3 summarizes the stakeholder attribution by mapping each stakeholder group to the corresponding design-type decisions and cross-design parameters used in the variance aggregation. We assign parameters on the basis of decision-making authority across the supply chain and project lifecycle. Infrastructure designers define infrastructure materials and vacuum-system specifications. Constructors make procurement decisions and oversee construction activities that govern supplier selection and construction-stage emissions. Pod designers choose the levitation concept and pod subsystem efficiencies. Operators set operating conditions and maintenance strategies that influence operational parameters and component service lives.

4. Results

4.1. GHG emissions of four hyperloop designs

Fig. 4(a) presents a component-wise breakdown of the mean GHG emissions for the four hyperloop design types. EDS systems produce higher emissions than EMS systems when paired with the same tube material. Concrete tubes, despite higher construction emissions, yield a lower overall footprint than steel tubes under both levitation types. Embodied emissions from infrastructure components dominate the total GHG footprint, followed by pod operation, construction, and vacuum operation. Within the infrastructure, rail is the largest contributor in concrete-tube systems, whereas tube emissions dominate for steel-tube designs. Fig. 4(b) illustrates the distribution of the total GHG footprint for each hyperloop design, where the shaded violins show the density of samples, the boxplots indicate median and interquartile range, and points represent individual simulations. Across all configurations, EMS-CT shows the lowest mean emissions with the narrowest distribution, whereas EDS-ST shows the highest mean emissions with the widest distribution.

Table 3
Stakeholder–parameter mapping for the variance attribution analysis. The continuous parameter indices are listed in Table 2.

	Design-type decision	Continuous parameter index	Parameter group description
Operators	None	22–31, 43–47	Replacement of components represented by component service lives; vacuum pressure inside the tube; operational profile, including occupancy, travel distance, pod operation speed, acceleration, and deceleration; operational electricity supplier
Pod designers	Levitation technology selection (EMS vs. EDS)	32–33, 35–42	Pod-design performance parameters, including motor efficiencies, pod mass, cooling system COP, regenerative braking efficiency, battery charge and discharge efficiencies, and aerodynamic heating share on the pod
Constructors	None	1–21	Embodied emissions of required materials via selecting the suppliers; construction activity emissions including transportation, prefabrication, and on-site construction; tube leakage rate
Infrastructure designers	Tube material selection (Concrete vs. Steel)	34	Vacuum pump efficiency

4.2. Variance contribution analysis for four hyperloop design types

Fig. 5 shows the component-wise GHG emissions variance contributions for the four hyperloop designs. Designs with concrete tubes exhibit lower total variance than their steel-tube counterparts, and EMS configurations consistently show less uncertainty than EDS systems. Across all designs, the use stage contributes the most to the total variance, while the construction stage (A4–5) contributes the least. This pattern is consistent across the four variants for two main reasons: (i) all variants are evaluated under the same functional unit, LCA boundary, stage definitions, and uncertainty assumptions, enabling direct comparison across designs; (ii) their GHG footprints are dominated by bulk materials and operational energy, as in other guideway transport systems [5,9,20].

Product-stage variances are smaller than those from the replacement stage (B4) for the same component because, compared to the uncertainty in service lives, the variance of material emission factors is relatively well-constrained in ecoinvent, as listed in Table 2. The replacement stage is therefore a major source of uncertainty. The overall variance is dominated by the service lives of tubes, rails, and pillars, whose high material demand is incurred repeatedly over the 100-year reference period. The service-life distributions determine the number of replacement cycles that occur and thus amplify uncertainty through service-life-based annualization of embodied impacts (see Equation (S1) in the supplementary material). Specifically, steel tubes generally contribute more variance than concrete tubes, and aluminum rails contribute more than steel rails. Pillars play a particularly important role because a failure of either the tube or the pillar is assumed to trigger reconstruction of the entire section. Given the higher construction-stage emissions of concrete-tube designs, this interdependency increases the pillar's variance contribution in B4 for EMS-CT and EDS-CT systems. These results highlight the importance of component durability and structural criticality in reducing replacement-stage uncertainty.

The construction stage (A4–5) contributes only a small share of the total variance across all designs, even though the associated parameters are modeled with broad uncertainty ranges. As detailed in Section S3 of the supplementary material, on-site construction energy is approximated by scaling viaduct and tunnel data from high-speed railways to hyperloop using uncertain scaling factors and tunnel share factors. These coarse assumptions indeed introduce substantial uncertainty at the activity level. However, once construction emissions are annualized over long structural lifetimes and normalized per passenger-kilometer, their absolute contribution to both the mean GHG emissions and the total variance becomes minor.

Fig. 6 presents the parameter-wise variance of GHG emissions in the operational energy stage across the four hyperloop design types. Overall, EMS systems display lower uncertainty than EDS systems. The three most influential parameters are vacuum pressure, the GHG intensity of electricity, and occupancy rate, followed by pod mass and cruise speed. Secondary contributors include motor efficiency, battery efficiencies, and the COP of the cooling system. In contrast, the impacts of regenerative braking efficiency, aerodynamic heating share, and vacuum pump efficiency are negligible. The variance contribution of occupancy rate differs between hyperloop designs with the same levitation technology but different tube materials. Since occupancy directly determines the

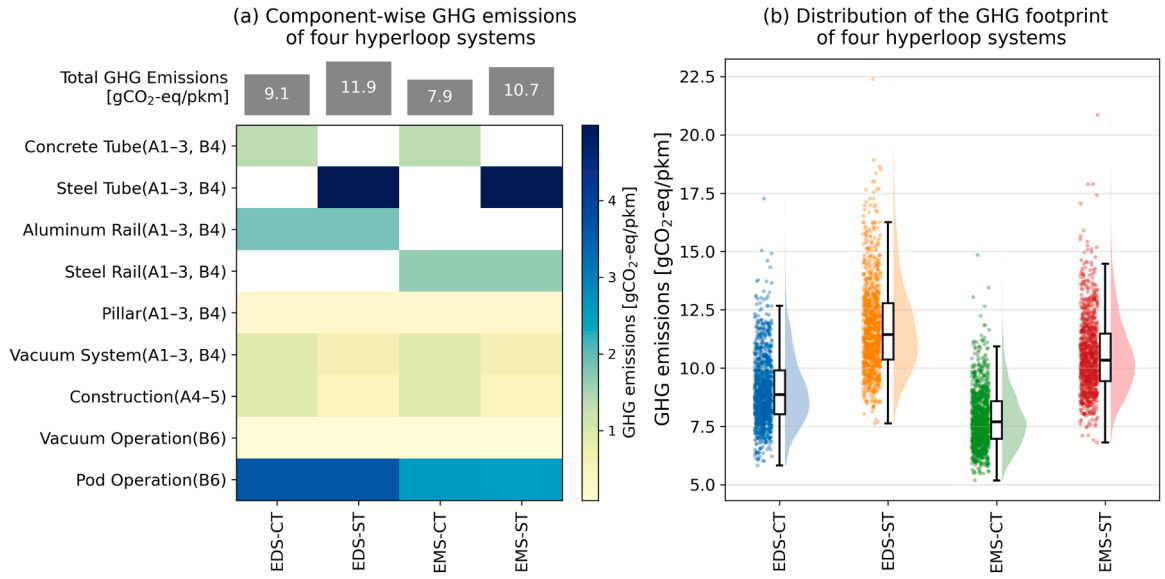

Fig. 4. (a) Component-wise mean GHG emissions for the four systems; grey bars show the total emissions for each design, and white cells indicate components that are not present in the corresponding configuration; (b) Distribution of the GHG footprint of four hyperloop systems. Updated visualization based on [62]. Note that the embodied GHG emissions from the pods are excluded in this study due to the lack of data.

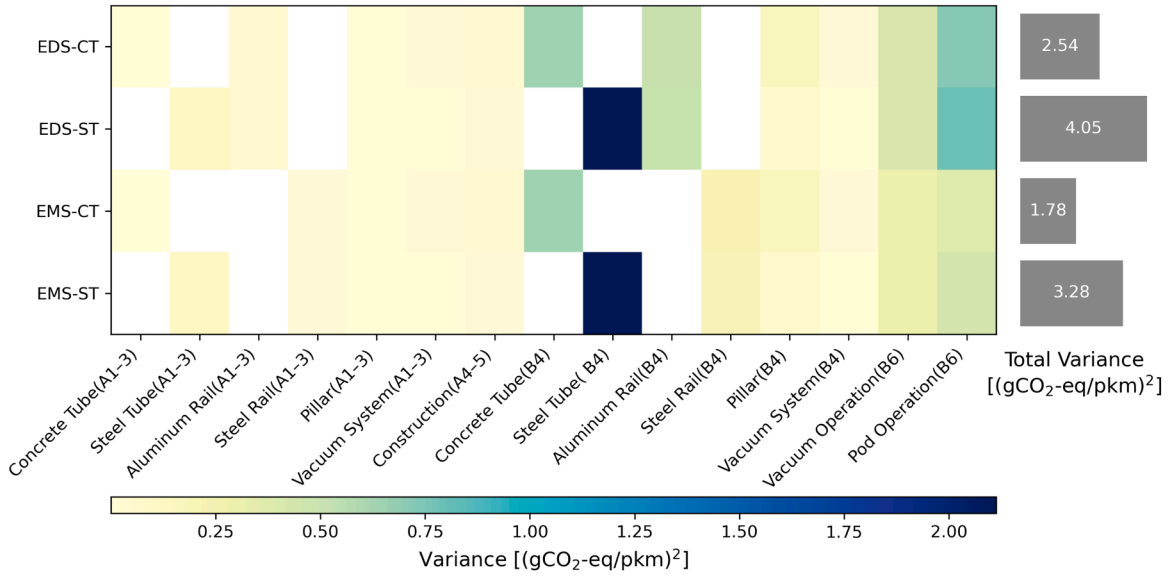

Fig. 5. Component-wise contributions to GHG emissions variance for the four hyperloop design types. Grey bars on the right show the total variance for each design, and white cells indicate components that are not present in the corresponding configuration. Note that the embodied GHG emissions from the pods are excluded in this study due to the lack of data.

number of annual transported passengers and inversely scales per-passenger emissions across all life-cycle stages, its impact is amplified in steel-tube systems. These systems have higher baseline emissions and are therefore more sensitive than concrete-tube systems to the same variation in occupancy.

Taken together, Figs. 5 and 6 show that extending component service lives and maintaining high operational efficiency are the primary levers for reducing both mean GHG emissions and their uncertainty, while the product-stage and construction-stage uncertainty play secondary roles.

4.3. Impact of stakeholder decisions on GHG emissions of hyperloops

Fig. 7 illustrates the contribution of each stakeholder group to the total GHG emissions variance. Operators have the greatest influence because they control over key operational parameters and affect component service life through maintenance strategies. Infrastructure designers rank second, primarily through their selection of tube material. Although they also determine vacuum pump efficiency, its contribution to total variance is negligible. Pod designers are the third most influential group by shaping emissions through levitation technology and key pod parameters such as mass, motor efficiency, and battery performance. However, due to limited data availability, the embodied emissions from pod manufacturing are not included in this study. Therefore, the variance contribution attributed to pod designers reflects only their influence on operational energy use and should be interpreted as a conservative lower bound. The implications of this omission are discussed in Section 5.1.4. Constructors contribute the least to overall uncertainty, with material supplier selection having a greater impact

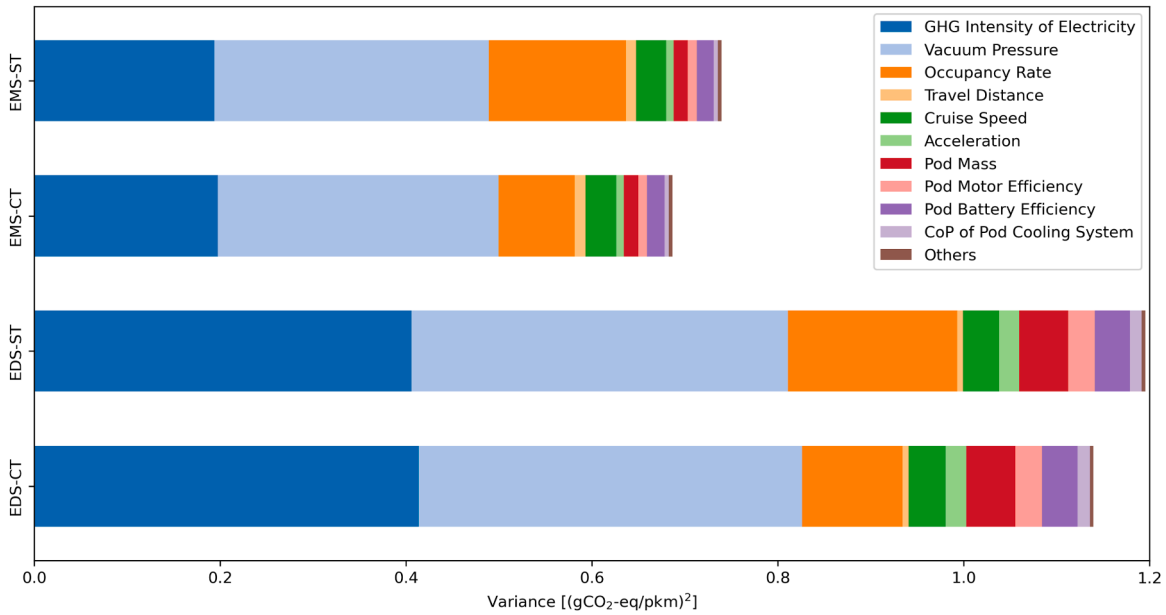

Fig. 6. Parameter-wise GHG emissions variance in LCA stage B6 for the four hyperloop design types.

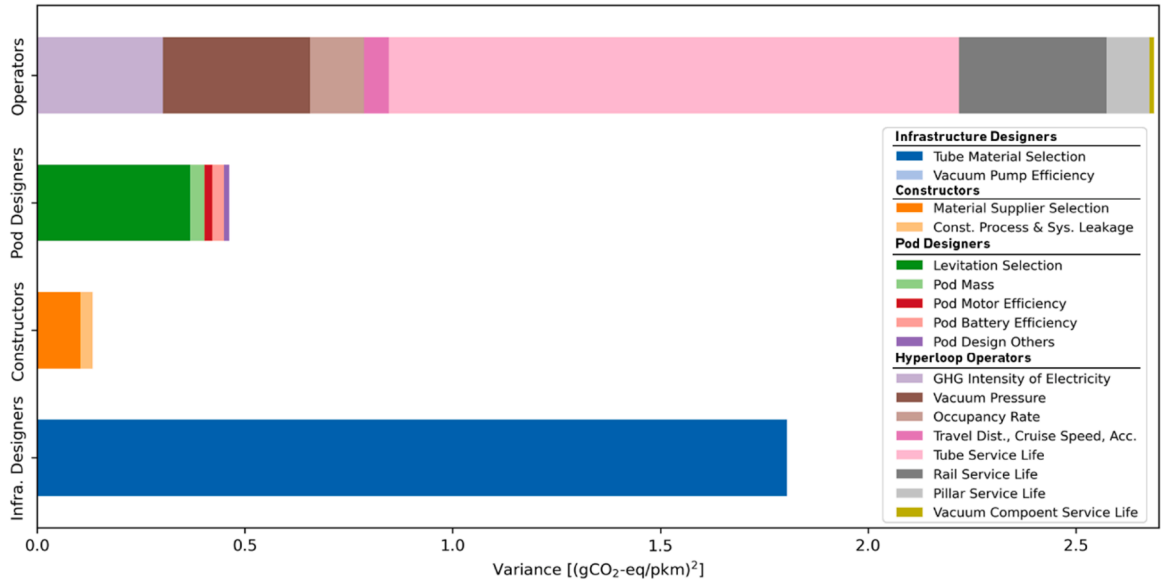

Fig. 7. Impact of stakeholder decisions on the GHG footprints of hyperloop systems. Note that the embodied GHG emissions from the pods are excluded in this study due to the lack of data.

than construction activities and vacuum leakage.

5. Discussion

This study addresses key gaps in the hyperloop LCA literature by jointly evaluating the effects of design-type decisions and cross-design parameters on GHG emissions. Conflicting findings in previous studies stem from inconsistent system boundaries and varying design assumptions. Our stochastic framework addresses these issues by applying a unified LCA boundary and comparing emissions and uncertainties across four hyperloop types. By integrating variance estimation for both design-type decisions and cross-design parameters, this decision-centric approach identifies the most impactful stakeholder decisions and supports coordinated strategies for reducing the hyperloop GHG footprint. Given the early-stage development of hyperloop and the lack of empirical data, this study has several limitations, which are discussed in the following section.

5.1. Modeling assumptions and limitations

5.1.1. Assumption of independence of inputs

This study assumes that all input variables are statistically independent so that variance contributions can be explicitly attributed to individual stakeholders. However, in practice, the decisions and parameters controlled by different stakeholders are not fully independent, as stakeholders typically work in coordinated project teams and their choices influence one another. For example, infrastructure designers may adapt tube materials or cross-sectional geometry in anticipation of operational requirements, while operators may adjust service patterns in response to design and construction constraints.

This independence assumption therefore neglects potential correlations among infrastructure design, construction, pod design, and operational decisions. As a result, the reported stakeholder variance contributions should thus be interpreted as approximate influences under independent decision-making, rather than as a full decomposition of system-wide, co-designed strategies. Future work could relax this assumption by introducing dependence structures, such as copulas or scenario-based joint decision sets, to capture coordinated decision-making and to quantify the stakeholder interactions in the variance attribution.

5.1.2. Parameter distribution selection

This framework uses probabilistic distributions to represent cross-design uncertainties more transparently than a deterministic LCA. Consequently, the plausibility of the selected distribution families and their parameters values directly affects both the estimated GHG footprint and the resulting uncertainty analysis.

We use uniform distributions when empirical data are unavailable, and expert judgment only provides plausible bounds rather than a reliable central tendency. In such cases, the uniform distribution is a maximum-entropy choice that assigns equal probability to all values within the specified range and therefore provides a conservative characterization of variance given the available information [63,64]. Consistent with established practice in uncertainty analysis for LCA studies [15,16,44,65], we apply this approach to operational and design parameters that are currently informed only by the early hyperloop literatures and expert judgment.

For the GHG emission factors, we use lognormal distributions based on the ecoinvent pedigree approach. The manufacturing processes for the materials, such as concrete, steel, and aluminum etc., are well understood, and their life cycle inventory data and pedigree matrices in ecoinvent have been validated against empirical data [26,66]. Prior work has shown that, under such conditions, epistemic uncertainty in the exact choice of distributional form has limited influence on product-stage LCA results [67]. We therefore follow common LCA practice and model these emission factors as lognormal distributions, focusing the uncertainty analysis on distribution parameters rather than on distribution-family ambiguity for well-characterized background processes.

For the service lives of the components, we derive their distributions from design lifespans and reliability studies of comparable civil structures. Previous studies indicate that Weibull and lognormal distributions represent the service lives of such structures well [38,40,68]. We calibrate these distributions by matching their means and coefficients of variation (COVs) to the data reported in the literature. This COV-matching approach has been shown to effectively capture the relevant uncertainty for comparative LCA uncertainty studies [15,16].

Overall, we select the parameter distributions to keep our study consistent with established practice in stochastic LCA of linear infrastructures. As empirical data on hyperloop components and operations become available, refining these distributions is expected to narrow the uncertainty ranges of those parameters. In particular, for parameters currently represented by uniform distributions in the construction and operational stages, replacing uniform distributions with more informative forms, such as lognormal or Gaussian, would concentrate probability around central values and reduce their variance contributions. Given the dominant contributions of the use stage and product stage to the mean GHG emissions and the comparatively small contribution of construction stage, this refinement is unlikely to change the qualitative stage ranking of the overall GHG footprint for the four studied hyperloop systems.

In the uncertainty analysis for the studied case, operators already emerge as the most influential stakeholder through their control of component service lives alone. Therefore, any reduction in the variance associated with parameters represented by uniform distributions, such as occupancy rate, travel distance, cruise speed, and acceleration and deceleration, is unlikely to alter their leading position. Pod designers are the mid-rank impactor as their choice of levitation technology induces a design-type variance that already exceeds the total variance attributed to constructors; accordingly, reducing the uncertainty of pod-related parameters modeled as uniform would not overturn this ordering. Therefore, the use of uniform distributions may conservatively inflate absolute variance magnitudes in a conservative way, but the main qualitative insights on the relative importance of life-cycle stages and stakeholder groups are expected to remain robust.

5.1.3. Simplified on-site construction modeling

Currently, data on the energy use and emissions of on-site construction for hyperloop infrastructure are unavailable. In this study, we therefore model the construction stage using a coarse proxy model based on scaled energy consumption for high-speed railway viaduct and tunnel construction, with data reported by [29]. As detailed in Section S3.3 in the supplementary material, we map hyperloop infrastructure to high-speed railways reference structures using scaling factors for viaduct and tunnel energy consumption, alongside an uncertain tunnel-length share factor. We assign broad uncertainty ranges to these parameters to explicitly account for both the lack of primary data and the structural differences between hyperloop and high-speed railway, making the construction-stage model conservative.

Even under these conservative assumptions, emissions from the construction stage remain relatively small compared with the embodied emissions of the bulk infrastructure materials, as shown in Fig. 4(a). When these emissions are annualized over long structural lifetimes and normalized per passenger-kilometer, the resulting contribution of the construction stage to overall variance is much smaller than that of the replacement and operational stages. Thus, although the simplified, analogy-based construction model clearly limits the precision of stage-specific conclusions regarding on-site construction, it does not materially overturn the identification of the dominant drivers of uncertainty at system level. However, the uncertainty associated with the construction stage should be interpreted as indicative rather than definitive in this study.

5.1.4. Omission of pod embodied GHG emissions

Another limitation of this study is the omission of the pod's embodied GHG emissions from the LCA boundary. This choice is primarily driven by data availability, as detailed bills of materials, manufacturing processes, and refurbishment or replacement strategies for hyperloop pods are not publicly available and are likely to remain highly design-specific at the early stage. Constructing a pod LCA from speculative component lists and generic vehicle analogues would introduce additional uncertainty that would be difficult to justify and interpret transparently. We therefore limit the study to infrastructure embodied and operational emissions.

Existing evidence suggests that this simplification has limited impact on the main conclusions. Prior studies on hyperloop and high-speed railways consistently show that infrastructure and operational energy dominate the life-cycle GHG footprint, whereas vehicle manufacturing contributes comparatively little [5,6,10,69–71]. This is because, in a long linear infrastructure, the mass of tubes, rails, and supporting structures per kilometer exceeds the in-service pod mass by several orders of magnitude. Even if pod designs exhibit substantial uncertainty in material choices and manufacturing routes, their total contribution to GHG emissions is expected to remain minor compared with the massive quantities of GHG-intensive materials, such as concrete and steel, required by the infrastructure. Accordingly, omitting the pod embodied emissions is unlikely to overturn the identification of infrastructure materials, service lives, and operational energy as the dominant contributors to both GHG emissions and associated variance.

Within the proposed stakeholder-attributed variance framework, this modeling choice implies that the influence of pod designers is captured only through operational and design decisions and parameters,

such as levitation technology, motor efficiency, and pod mass, etc., and not through pod manufacturing or pod refurbishment. Their attributed contribution should therefore be interpreted as a conservative lower bound, and the inferred influence of infrastructure designers and operators may be slightly overstated relative to a model that includes the embodied emissions of pods. However, even if embodied emissions of pods were included, their overall contribution would still be constrained by their comparatively small share of the system GHG footprint. Meanwhile, operators control parameters that govern service life and operational efficiency, and infrastructure designers determine the materials used in the infrastructure, both of which affect significantly larger emission stocks. Thus, including pod manufacturing would unlikely allow pod designers to overtake operators or infrastructure designers in the stakeholder ranking in the studied case. As data availability improves, future work should incorporate dedicated pod LCAs for different levitation technologies and service-life scenarios, thereby expanding the system boundary and refining the stakeholder rankings.

5.2. *Future scenario in 2050*

Hyperloop remains at an early design stage, and any large-scale deployment would likely occur in a future energy system with lower background GHG intensities than those of today. In this section, we estimate the mean GHG footprint and the relative ranking of the four hyperloop design variants under a projected 2050 decarbonization scenario by scaling the emission factors with projected reduction ratios for the embodied emissions of materials and operational electricity derived from literature. In this scenario analysis, we keep the assumption of service lives unchanged and apply the scaling only to the mean emission factors for materials, electricity, and construction.

Zhang et al. [72] modeled future embodied emissions using the Integrated Model to Assess the Global Environment (IMAGE) under Representative Concentration Pathway (RCP) of 1.9 W/m^2 (1.5 °C scenario by 2050) and reported substantial reductions: 70 % for concrete, 54 % for steel, and 19 % for aluminum. Similarly, Beckert et al. [5] estimated a 45 % drop in the GHG intensity of electricity. Consistent with these studies, we applied the same reductions to the emission factors of the above parameters in our analysis for 2050. For consistency and to maintain a conservative outlook, we assumed a 45 % reduction in construction emissions, although full electrification of construction machinery by 2050 could enable larger reductions.

Fig. 8 compares the GHG footprints of the four hyperloop design variants under current emission factors and under the 2050 decarbonization scenario defined above. Compared with the 2025 baseline, the mean footprint decreases by 43.8 % for EDS-CT, 45.6 % for EDS-ST, 51.7 % for EMS-CT, and 51.6 % for EMS-ST. The four hyperloop variants exhibit similar reduction ratios because, although the 2050 scenario applies different decarbonization factors to different materials, the variants share several major materials and rely on the same operational electricity mix. Since these common inputs dominate their baseline footprints, the resulting percentage reductions are of similar magnitude across all designs. However, the EMS variants benefit more because they require steel rails and therefore have a larger share of the projected reduction in embodied emissions of steel, whereas the EDS variants rely on aluminum rails whose projected reduction is smaller. Despite these differences in reduction ratios, the overall ranking of contributions remains unchanged, and infrastructure-related emissions continue to exceed operational emissions across all variants in the projected 2050 scenario.

If the GHG emissions of materials and electricity decline down under the 2050 scenario while the component service-life distributions remain unchanged, the relative variance contribution of service-life would be

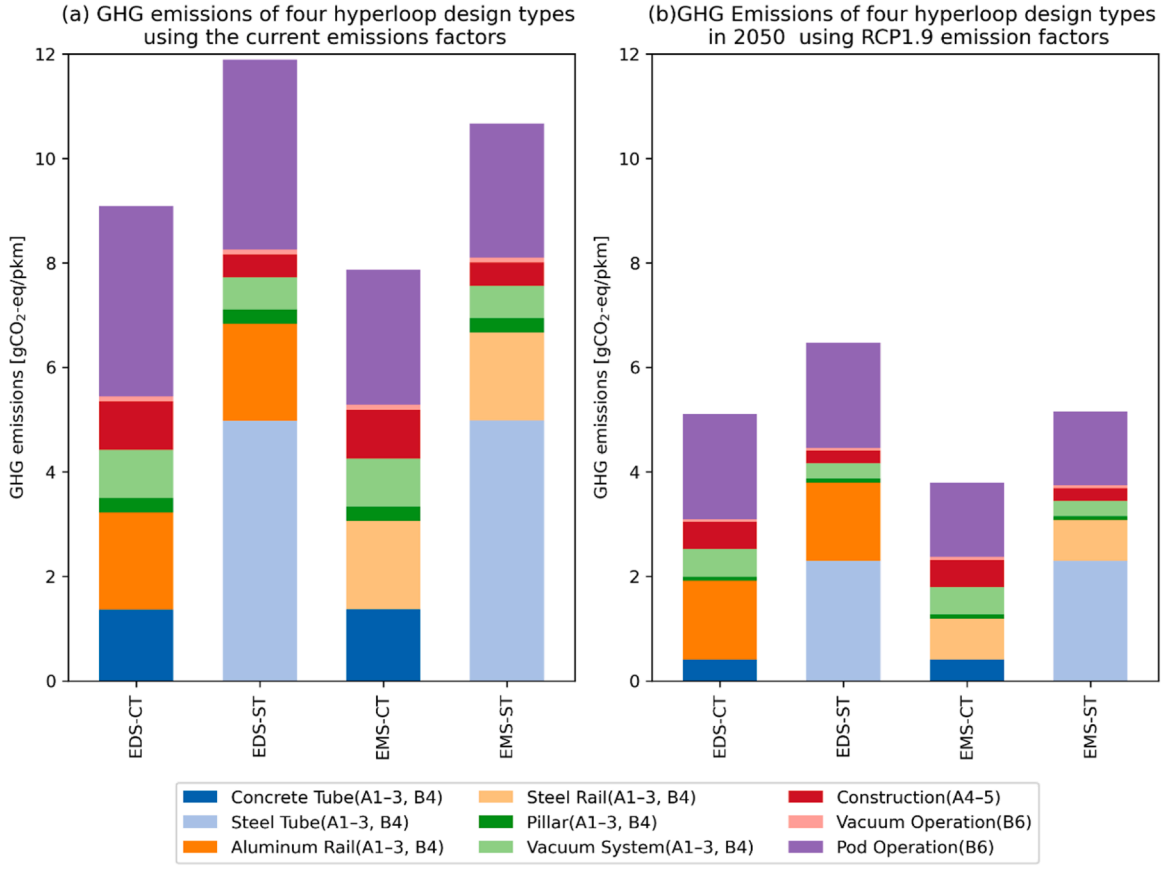

Fig. 8. GHG emissions of four hyperloop design types: (a) using current factors, (b) using factors predicted for 2050 based on RCP1.9. Note that the embodied GHG emissions from the pods are excluded in this study due to the lack of data.

more pronounced. This indicates that, in addition to decarbonizing materials and electricity, choosing durable structural materials and implementing maintenance strategies that extend component service lives will be key levers for reducing the future GHG footprint of hyperloop systems.

5.3. Case-dependent findings and general recommendations for stakeholders

The input parameters in this study fall into two groups: context-specific parameters tied to the Zurich–Geneva case and Swiss conditions, and generic parameters intended to represent hyperloop technology more broadly. To reduce dependence on a single case length, we model travel distance using a uniform distribution between 100 and 600 km; and the results can therefore be interpreted as representative of medium- to long-distance intercity connections rather than of one fixed route. By contrast, the hourly profile of daily passenger demand, the occupancy rate, and the region-specific emission factors for electricity and materials are case-specific. For example, lower demand or lower occupancy rate substantially increases the GHG footprint because both parameters appear in the denominator of the functional unit (see Equation (S1) in the Supplementary Material), which is defined as transporting one passenger over 1 km over a 100-year system lifetime.

Beyond demand and occupancy, the regional supply context also shapes the results. The background emission factors in the inventory can be partitioned into locally supplied inputs and globally traded inputs. Locally supplied inputs reflect regional energy systems and construction supply chains and therefore vary strongly across contexts, most notably the GHG intensity of electricity and, to a lesser extent, concrete. By contrast, many other materials and components are typically sourced through global markets, such as steel and aluminum, and therefore exhibit comparatively smaller regional variation. This distinction helps identify which case-specific assumptions are most likely to alter the dominant life-cycle contributors and stakeholder rankings.

To illustrate how locally supplied inputs condition case-specific conclusions, we consider a high-carbon-grid context such as northern India. Compared with the Zurich–Geneva case, the electricity emission factor can increase from about 0.00909 to 1.28 kg CO_2-eq/kWh, whereas the concrete emission factor increases more modestly from about 368 to 408 kg CO_2-eq/m^3 [23]. Under such a shift, emissions from the operational electricity would likely overtake embodied infrastructure emissions as the dominant contributor to the life-cycle footprint. Meanwhile, parameters and decisions that affect operational electricity demand, such as pod efficiency, mass, propulsion performance, and operating conditions, would exert greater impact on both mean emissions and uncertainty. Therefore, the numerical stage contributions and stakeholder rankings reported in this study should be interpreted as context-dependent, particularly with respect to the regional electricity mix and demand conditions.

Several insights are nevertheless expected to remain robust across different contexts. Across the four studied configurations, the EMS-CT design is structurally favorable because it combines two generic advantages: concrete typically has lower embodied GHG emissions than steel for equivalent structural performance, and EMS levitation currently achieves higher efficiency than EDS. At the stakeholder level, operators are expected to remain among the most influential groups because they control high-leverage factors such as occupancy, electricity procurement, and maintenance strategies that determine component service lives. Infrastructure designers are also expected to remain highly influential in most contexts because they determine the material composition of the resource-intensive guideway. Pod designers are also likely to remain a mid-ranked contributors in low-carbon electricity contexts, but their influence can increase in high-carbon-grid regions where operational electricity dominates making pod efficiency parameters more decisive. By contrast, constructors are structurally secondary because construction activities contribute the smallest share of the normalized footprint and variance in the studied designs, despite the associated parameter are modeled with wide uncertainty ranges.

Building on these general insights, we derive stakeholder-specific decarbonization strategies that remain applicable across diverse contexts. Operators should implement robust inspection and maintenance regimes to extend the service lives of major structures and should pursue high occupancy and low-carbon electricity procurement through demand-responsive scheduling and engagement with energy providers. They also should try to maintain the vacuum around 100 Pa inside the tube, as the GHG emissions from the vacuum assurance are much smaller than GHG emissions from overcoming the pod's air resistance. Infrastructure designers should prioritize concrete tubes over steel wherever structural and geometric constraints allow and should design guideway components for maintainability and long service life, thereby reducing both mean emissions and associated uncertainty. Pod designers should select EMS levitation when compatible with system requirements and minimize pod energy demand through low-mass vehicle concepts and high-efficiency propulsion and charging systems. The main decarbonization lever for constructors is to select low-carbon suppliers for the a given material. Together, these recommendations target the most influential levers identified by this stochastic LCA study, while acknowledging that the quantitative benefits will vary with case-specific demand profiles and background electricity and material mixes.

6. Conclusion

This study introduces a stochastic, parametric LCA framework with integrated uncertainty quantification that resolves key discrepancies in earlier hyperloop research. By unifying uncertainties from both design-type choices and cross-design parameters within a single variance-estimation structure, the framework identifies the most influential parameters and attributes them to the corresponding stakeholder groups across all life-cycle stages.

Applied to four representative hyperloop configurations for the Zurich–Geneva case, the framework shows that embodied emissions of the infrastructure and the pod operations dominate the mean GHG emissions of hyperloop systems, with the EMS-CT variant yielding the lowest expected GHG footprint and EDS-ST the highest. Component service lives emerge as the largest single source of uncertainty, while operational parameters collectively exert a comparable influence on variance. These quantitative rankings are case-specific as they depend on the Zurich–Geneva demand profile and Swiss supply chains. However, the structural finding that long-lived infrastructure materials and operational performance jointly dominate the footprint is expected to hold across contexts.

Overall, the proposed framework supports decision-centric, low-carbon design by linking emissions uncertainty to the actors who shape it. This enables more targeted and effective decarbonization strategies for emerging transport systems such as hyperloop systems. Future work should extend the analysis by incorporating pod embodied emissions, broadening the set of environmental indicators, refining distributional assumptions as empirical data on hyperloop become available, and relaxing the current independence assumption by introducing dependence structures to capture coordinated decision-making and its effects on variance attribution.

Data availability statement

All parameter values used in the stochastic LCA models are reported in the main article and in the supplementary material. Part of these data are based on internal design data and experimental estimates provided by EuroTube. Due to commercial confidentiality, the underlying raw EuroTube design and experimental datasets are not publicly available but can be requested from the EuroTube co-authors or the corresponding author and may be shared under reasonable conditions and subject to EuroTube's approval.

Declaration of generative AI and AI- assisted technologies in the writing process

During the preparation of this work the authors used ChatGPT to improve readability and language. After using this tool, the authors reviewed and edited the content as needed and take full responsibility for the content of the publication.

CRediT authorship contribution statement

Jianxiang Ma: Writing – original draft, Visualization, Validation, Methodology, Investigation, Formal analysis, Data curation, Conceptualization. **Jianpeng Cao:** Writing – review & editing, Validation, Project administration, Methodology, Formal analysis. **Lorenzo Benedetti:** Writing – review & editing, Validation, Resources, Data curation. **Zienab Elghoul:** Writing – review & editing, Visualization, Resources. **Guillaume Habert:** Writing – review & editing, Validation, Supervision, Methodology, Funding acquisition, Conceptualization.

Declaration of competing interest

The authors declare that they have no known competing financial interests or personal relationships that could have appeared to influence the work reported in this paper.

Acknowledgements

The research presented in this article was conducted within the research project "Smart Mobile Factory for Infrastructure Projects (SMF4INFRA)", which has received funding from the Swiss National Science Foundation under grant agreement No. 204852. The authors are grateful to Dr. Fernanda Belizario-Silva from the Chair of Sustainable Construction at ETH Zurich and colleagues from EuroTube Foundation for their support in this project.

Supplementary materials

Supplementary material associated with this article can be found, in the online version, at doi:10.1016/j.rineng.2026.110561.

References

[1] IEA, CO2 Emissions overview of transport sector [WWW Document]. https://www.iea.org/energy-system/transport, 2023 accessed 1.12.25.
[2] IEA, CO2 Emissions overview of aviation [WWW Document]. https://www.iea.org/energy-system/transport/aviation, 2023 accessed 1.12.25.
[3] A. Odenweller, F. Ueckerdt, G.F. Nemet, M. Jensterle, G. Luderer, Probabilistic feasibility space of scaling up green hydrogen supply, Nat. Energy 7 (2022) 854–865, https://doi.org/10.1038/s41560-022-01097-4.
[4] F. Ueckerdt, C. Bauer, A. Dirnaichner, J. Everall, R. Sacchi, G. Luderer, Potential and risks of hydrogen-based e-fuels in climate change mitigation, Nat. Clim. Change 11 (2021) 384–393, https://doi.org/10.1038/s41558-021-01032-7.
[5] P. Beckert, G. Pareschi, J. Ehwald, R. Sacchi, C. Bauer, Fast as a plane, clean as a train? Prospective life cycle assessment of a hyperloop system, Resour. Environ. Sustain. 17 (2024) 100162, https://doi.org/10.1016/j.resenv.2024.100162.
[6] Pareschi, G., Ehwald, J., Leng, N., Beckert, P., Guo, B., 2023. Potential analysis for vacuum transport technologies in public transport in Switzerland: life-cycle analysis with focus on energy consumption and environmental impact of a vacuum transport infrastructure. https://doi.org/10.13140/RG.2.2.22012.76169.
[7] A.E. Scholz, D. Trifonov, M. Hornung, Environmental life cycle assessment and operating cost analysis of a conceptual battery hybrid-electric transport aircraft, CEAS Aeronaut. J. 13 (2022) 215–235, https://doi.org/10.1007/s13272-021-00556-0.
[8] EuroTube Foundation, EuroTube – Hyperloop [WWW Document], EuroTube. URL, https://eurotube.org/hyperloop/, 2024. accessed 1.12.25.
[9] J.K. Nøland, Prospects and challenges of the Hyperloop Transportation System: a systematic technology review, IEEE Access 9 (2021) 28439–28458, https://doi.org/10.1109/ACCESS.2021.3057788.
[10] Beckert, P., 2022. Life cycle assessment of a high-speed vacuum transport system (Hyperloop). https://doi.org/10.13140/RG.2.2.28255.33440/1.
[11] F. Liu, M. Shafique, X. Luo, Literature review on life cycle assessment of transportation alternative fuels, Environ. Technol. Innov. 32 (2023) 103343, https://doi.org/10.1016/j.eti.2023.103343.
[12] L. Mitropoulos, A. Kortsari, A. Koliatos, G. Ayfantopoulou, The hyperloop system and stakeholders: a review and future directions, Sustainability 13 (2021) 8430, https://doi.org/10.3390/su13158430.
[13] W. Zhang, Y. Li, H. Li, S. Liu, J. Zhang, Y. Kong, Systematic review of life cycle assessments on carbon emissions in the transportation system, Environ. Impact Assess. Rev. 109 (2024) 107618, https://doi.org/10.1016/j.eiar.2024.107618.
[14] M. Landgraf, A. Horvath, Embodied greenhouse gas assessment of railway infrastructure: the case of Austria, Environ. Res. Infrastruct. Sustain. 1 (2021) 025008, https://doi.org/10.1088/2634-4505/ac1242.
[15] O. Larsson Ivanov, D. Honfi, F. Santandrea, H. Stripple, Consideration of uncertainties in LCA for infrastructure using probabilistic methods, Struct. Infrastruct. Eng. 15 (2019) 711–724, https://doi.org/10.1080/15732479.2019.1572200.
[16] Larsson Ivanov, O., Honfi, D., Stripple, H., 2018. Uncertainty and variation in LCA.
[17] E. Musk, Hyperloop Alpha, SpaceX and Tesla Motors (2013).
[18] M. Janić, Multicriteria evaluation of the high speed rail, transrapid maglev and hyperloop systems, Transp. Syst. Technol. 4 (2018) 5–31, https://doi.org/10.17816/transsyst2018445-31.
[19] M. Janić, Estimation of direct energy consumption and CO2 emission by high speed rail, transrapid maglev and hyperloop passenger transport systems, Int. J. Sustain. Transp. 15 (2021) 696–717, https://doi.org/10.1080/15568318.2020.1789780.
[20] A. Hirde, A. Khardenavis, R. Banerjee, M. Bose, V.S.S. Pavan Kumar Hari, Energy and emissions analysis of the hyperloop transportation system, Environ. Dev. Sustain. 25 (2023) 8165–8196, https://doi.org/10.1007/s10668-022-02393-5.
[21] A. Nurdiawati, B.A. Mir, S.G. Al-Ghamdi, Recent advancements in prospective life cycle assessment: current practices, trends, and implications for future research, Resour. Environ. Sustain. 20 (2025) 100203, https://doi.org/10.1016/j.resenv.2025.100203.
[22] Technical Committee CEN/TC 350, 2012. Sustainability of construction works – assessment of environmental performance of buildings – Calculation method.
[23] G. Wernet, C. Bauer, B. Steubing, J. Reinhard, E. Moreno-Ruiz, B. Weidema, The ecoinvent database version 3 (part I): overview and methodology, Int. J. Life Cycle Assess 21 (2016) 1218–1230, https://doi.org/10.1007/s11367-016-1087-8.
[24] K. Decker, J. Chin, A. Peng, C. Summers, G. Nguyen, A. Oberlander, G. Sakib, N. Sharifrazi, C. Heath, J.S. Gray, R.D. Falck, Conceptual sizing and feasibility study for a magnetic plane concept, in: 55th AIAA Aerospace Sciences Meeting, AIAA SciTech Forum, American Institute of Aeronautics and Astronautics, 2017, https://doi.org/10.2514/6.2017-0221.
[25] Intergovernmental Panel on Climate Change (IPCC), Climate Change 2021 – The Physical Science Basis: Working Group I Contribution to the Sixth Assessment Report of the Intergovernmental Panel on Climate Change, Cambridge University Press, Cambridge, 2023, https://doi.org/10.1017/9781009157896.
[26] A. Ciroth, S. Muller, B. Weidema, P. Lesage, Empirically based uncertainty factors for the pedigree matrix in ecoinvent, Int. J. Life Cycle Assess. 21 (2016) 1338–1348, https://doi.org/10.1007/s11367-013-0670-5.
[27] B. Weidema, C. Bauer, R. Hischier, Data quality guideline for the ecoinvent database version 3. [R], Overv. Methodol. Ecoinvent Rep. 1 St Gallen Ecoinvent Cent. (2013) 76–84.
[28] C. Mutel, Brightway: an open source framework for Life cycle assessment, J. Open Source Softw. 2 (2017) 236, https://doi.org/10.21105/joss.00236.
[29] Y. Chang, S. Lei, J. Teng, J. Zhang, L. Zhang, X. Xu, The energy use and environmental emissions of high-speed rail transportation in China: a bottom-up modeling, Energy 182 (2019) 1193–1201, https://doi.org/10.1016/j.energy.2019.06.120.
[30] A. De Bortoli, L. Bouhaya, A. Feraille, A life cycle model for high-speed rail infrastructure: environmental inventories and assessment of the Tours-Bordeaux railway in France, Int. J. Life Cycle Assess. 25 (2020) 814–830, https://doi.org/10.1007/s11367-019-01727-2.
[31] A. Kortazar, G. Bueno, D. Hoyos, Environmental balance of the high speed rail network in Spain: a life cycle assessment approach, Res. Transp. Econ. 90 (2021) 101035, https://doi.org/10.1016/j.retrec.2021.101035.
[32] J.-Y. Lee, C.-K. Lee, Y.-Y. Chun, Greenhouse gas emissions from high-speed rail infrastructure construction in Korea, Transp. Res. Part Transp. Environ. 87 (2020) 102514, https://doi.org/10.1016/j.trd.2020.102514.
[33] J. Cao, I. Č, ustović, R. Soman, D. Hall, Reinforcement learning for smart mobile factory operation in linear infrastructure projects, in: Int. Symp. Autom. Robot. Constr. ISARC Proc. 2024 Proceedings of the 41st ISARC, 2024, pp. 738–744, https://doi.org/10.22260/ISARC2024/0096. Lille, France.
[34] P. Dallasega, I. Kaushal, A. Revolti, N. Miori, Life cycle analysis for the concept design of a smart mobile factory (SMF) for infrastructure construction projects, in: M. Thürer, R. Riedel, G. von Cieminski, D. Romero (Eds.), Advances in Production Management Systems. Production Management Systems for Volatile, Uncertain, Complex, and Ambiguous Environments, Springer Nature Switzerland, Cham, 2024, pp. 33–47, https://doi.org/10.1007/978-3-031-71637-9_3.
[35] P. Dallasega, A. Revolti, F. Schulze, L. Benedetti, D. de Morsier, Requirement analysis and concept design of a smart mobile factory for infrastructure projects, in: E. Alfnes, A. Romsdal, J.O. Strandhagen, G. von Cieminski, D. Romero (Eds.), Advances in Production Management Systems. Production Management Systems for Responsible Manufacturing, Service, and Logistics Futures, IFIP Advances in Information and Communication Technology, Springer Nature Switzerland, Cham, 2023, pp. 19–33, https://doi.org/10.1007/978-3-031-43670-3_2.
[36] J. Ma, A. Revolti, L. Benedetti, E.Z. Escamilla, G. Habert, Emission-based relocation strategies for mobile prefabrication factories, in: M. Kioumarsi, B. Shafei (Eds.), The 1st International Conference on Net-Zero Built Environment, Springer Nature Switzerland, Cham, 2025, pp. 1687–1698, https://doi.org/10.1007/978-3-031-69626-8_140.

[37] K. Goulouti, P. Padey, A. Galimshina, G. Habert, S. Lasvaux, Uncertainty of building elements' service lives in building LCA & LCC: what matters? Build. Environ. 183 (2020) 106904 https://doi.org/10.1016/j.buildenv.2020.106904.
[38] M.F.D. Morales, A. Passuello, A.P. Kirchheim, R.J. Ries, Monte Carlo parameters in modeling service life: influence on life-cycle assessment, J. Build. Eng. 44 (2021) 103232, https://doi.org/10.1016/j.jobe.2021.103232.
[39] A. Silva, J. De Brito, P.L. Gaspar, Methodologies for Service Life Prediction of Buildings, Green Energy and Technology, Springer International Publishing, Cham, 2016, https://doi.org/10.1007/978-3-319-33290-1.
[40] J. Wang, Reliability Analysis and Data Driven Modelling of Railway Component Failure, Nanyang Technological University, 2021, https://doi.org/10.32657/10356/159237.
[41] C. Kang, S. Schneider, M. Wenner, S. Marx, Experimental investigation on the fatigue behaviour of rails in the transverse direction, Constr. Build. Mater. 272 (2021) 121666, https://doi.org/10.1016/j.conbuildmat.2020.121666.
[42] C. Kang, S. Schneider, M. Wenner, S. Marx, Experimental investigation on rail fatigue resistance of track/bridge interaction, Eng. Struct. 216 (2020) 110747, https://doi.org/10.1016/j.engstruct.2020.110747.
[43] J.M. van Noortwijk, H.E. Klatter, The use of lifetime distributions in bridge maintenance and replacement modelling, Comput. Struct., Adv. Probabilistic Mech. Struct. Reliability 82 (2004) 1091–1099, https://doi.org/10.1016/j.compstruc.2004.03.013.
[44] G. Vignali, Ballasted or ballastless for a railway infrastructure? A comparative environmental impact assessment of two solutions, Clean. Environ. Syst. 12 (2024) 100158, https://doi.org/10.1016/j.cesys.2023.100158.
[45] M. Puig Arnavat, S. Soprani, M. Søgaard, K. Engelbrecht, J. Ahrenfeldt, U. Henriksen, P. Vang Hendriksen, Integration of mixed conducting membranes in an oxygen–steam biomass gasification process, RSC Adv. 3 (2013), https://doi.org/10.1039/c3ra44509g.
[46] M. Bizzozero, Y. Sato, M.A. Sayed, Aerodynamic study of a Hyperloop pod equipped with compressor to overcome the Kantrowitz limit, J. Wind Eng. Ind. Aerodyn. 218 (2021) 104784, https://doi.org/10.1016/j.jweia.2021.104784.
[47] X. Chen, L. Zhao, J. Ma, Y. Liu, Aerodynamic simulation of evacuated tube maglev trains with different streamlined designs, J. Mod. Transp. 20 (2012) 115–120, https://doi.org/10.1007/BF03325788.
[48] J.-S. Oh, T. Kang, S. Ham, K.-S. Lee, Y.-J. Jang, H.-S. Ryou, J. Ryu, Numerical analysis of aerodynamic characteristics of hyperloop system, Energies 12 (2019) 518, https://doi.org/10.3390/en12030518.
[49] Y. Seo, M. Cho, D.H. Kim, T. Lee, J. Ryu, C. Lee, Experimental analysis of aerodynamic characteristics in the Hyperloop system, Aerosp. Sci. Technol. 137 (2023) 108265, https://doi.org/10.1016/j.ast.2023.108265.
[50] M. Flankl, T. Wellerdieck, A. Tüysüz, J.W. Kolar, Scaling laws for electrodynamic suspension in high-speedtransportation, IET Electr. Power Appl. 12 (2018) 357–364, https://doi.org/10.1049/iet-epa.2017.0480.
[51] C. Timperio, Linear Induction Motor (LIM) for Hyperloop Pod Prototypes, ETH Zurich, Zurich, Switzerland, 2018.
[52] J. Maier, C. Marggraf-Micheel, F. Zinn, T. Dehne, J. Bosbach, Ceiling-based cabin displacement ventilation in an aircraft passenger cabin: analysis of thermal comfort, Build. Environ. 146 (2018) 29–36, https://doi.org/10.1016/j.buildenv.2018.09.031.
[53] P. Moreno, C. Solé, A. Castell, L.F. Cabeza, The use of phase change materials in domestic heat pump and air-conditioning systems for short term storage: a review, Renew. Sustain. Energy Rev. 39 (2014) 1–13, https://doi.org/10.1016/j.rser.2014.07.062.
[54] A.P. Johnson, P. Andrew, High Speed Linear Induction Motor Efficiency Optimization (Thesis), Massachusetts Institute of Technology, 2005.
[55] Baudin, M., Dutfoy, A., Iooss, B., Popelin, A.-L., 2015. Open TURNS: an industrial software for uncertainty quantification in simulation. pp. 1–38. https://doi.org/10.1007/978-3-319-11259-6_64-1.
[56] P. Virtanen, R. Gommers, T.E. Oliphant, M. Haberland, T. Reddy, D. Cournapeau, E. Burovski, P. Peterson, W. Weckesser, J. Bright, S.J. van der Walt, M. Brett, J. Wilson, K.J. Millman, N. Mayorov, A.R.J. Nelson, E. Jones, R. Kern, E. Larson, C. J. Carey, İ. Polat, Y. Feng, E.W. Moore, J. VanderPlas, D. Laxalde, J. Perktold, R. Cimrman, I. Henriksen, E.A. Quintero, C.R. Harris, A.M. Archibald, A.H. Ribeiro, F. Pedregosa, P. van Mulbregt, SciPy 1.0: fundamental algorithms for scientific computing in Python, Nat. Methods 17 (2020) 261–272, https://doi.org/10.1038/s41592-019-0686-2.
[57] A. Saltelli (Ed.), Sensitivity Analysis in practice: a Guide to Assessing Scientific Models, Wiley, Hoboken, NJ, 2004.
[58] Sudret, B., 2007. Uncertainty propagation and sensitivity analysis in mechanical models – contributions to structural reliability and stochastic spectral methods.
[59] A. Prokopov, B.A. Olsson, S.M. Famurewa, M. Rantatalo, Selection of track form in railway tunnel from a life cycle analysis perspective, Int. J. Syst. Assur. Eng. Manag. (2024), https://doi.org/10.1007/s13198-024-02423-7.
[60] Hardt Hyperloop Inc., Hyperloop system description [WWW Document], URL, https://docs.hardt.global/what-is-hyperloop/hyperloop-system-description, 2025. accessed 1.11.25.
[61] E. Apostolaki-Iosifidou, P. Codani, W. Kempton, Measurement of power loss during electric vehicle charging and discharging, Energy 127 (2017) 730–742, https://doi.org/10.1016/j.energy.2017.03.015.
[62] J. Ma, L. Benedetti, E.Z. Escamilla, G. Habert, Impact of component service life uncertainty on the embodied carbon emissions of hyperloop infrastructure, in: C. D'Erme, C. Paglia, E. Giner Cordero (Eds.), Proceedings of the RILEM Spring Convention and Conference 2025, RILEM Bookseries, Springer Nature Switzerland, Cham, 2026, pp. 293–302, https://doi.org/10.1007/978-3-032-14170-5_29.
[63] E.T. Jaynes, Information theory and Statistical mechanics, Phys. Rev. 106 (1957) 620–630, https://doi.org/10.1103/PhysRev.106.620.
[64] C. Soize, Maximum entropy approach for modeling random uncertainties in transient elastodynamics, J. Acoust. Soc. Am. 109 (2001) 1979–1996, https://doi.org/10.1121/1.1360716.
[65] Z. Barahmand, M.S. Eikeland, Life cycle Assessment under uncertainty: a scoping review, World 3 (2022) 692–717, https://doi.org/10.3390/world3030039.
[66] M. van der Spek, A. Ramirez, A. Faaij, Improving uncertainty evaluation of process models by using pedigree analysis. A case study on CO2 capture with monoethanolamine, Comput. Chem. Eng. 85 (2016) 1–15, https://doi.org/10.1016/j.compchemeng.2015.10.006.
[67] H. AzariJafari, G. Guest, R. Kirchain, J. Gregory, B. Amor, Towards comparable environmental product declarations of construction materials: insights from a probabilistic comparative LCA approach, Build. Environ. 190 (2021) 107542, https://doi.org/10.1016/j.buildenv.2020.107542.
[68] K. Goulouti, D. Favre, M. Giorgi, P. Padey, A. Galimshina, G. Habert, S. Lasvaux, Dataset of service life data for 100 building elements and technical systems including their descriptive statistics and fitting to lognormal distribution, Data Brief 36 (2021) 107062, https://doi.org/10.1016/j.dib.2021.107062.
[69] C.E.S. Andrade de, M.de A. D'Agosto, Energy use and carbon dioxide emissions assessment in the lifecycle of passenger rail systems: the case of the Rio de Janeiro Metro, J. Clean. Prod. 126 (2016) 526–536, https://doi.org/10.1016/j.jclepro.2016.03.094.
[70] H. Kato, N. Shibahara, M.K. Co, M. Osada, Y. Hayashi, A life cycle assessment for evaluating environmental impacts of inter-regional high-speed mass transit projects, J. East. Asia Soc. Transp. Stud. 6 (2005) 3211–3224.
[71] Matthias Tuchschmid, Wolfram Knörr, Alexander Schacht, Moritz Mottschall, Martin Schmied, 2011. Carbon footprint and environmental impact of railway In frastructure (Technical Report). International Union of Railways.
[72] X. Zhang, N. Heeren, C. Bauer, P. Burgherr, R. McKenna, G. Habert, The impacts of future sectoral change on the greenhouse gas emissions of construction materials for Swiss residential buildings, Energy Build. 303 (2024) 113824, https://doi.org/10.1016/j.enbuild.2023.113824.